Original Contributions

Incorporating Mouse Genome
Mammalian Genome
Genes and Phenotypes

# Genetic and phenotypic analysis of the mouse mutant *mh*$^{2J}$, an *Ap3d* allele caused by IAP element insertion

**Prameela Kantheti,[1] Maria E. Diaz,[2] Andrew Peden,[3] Eunju Seong,[1,4] David F. Dolan,[4,5] Margaret S. Robinson,[3] Jeffrey L. Noebels,[2] and Margit Burmeister[1,4,6]**

[1]Mental Health Research Inst., University of Michigan, 205 Zina Pitcher Place, Ann Arbor, Michigan 48109-0720, USA
[2]Dept of Neurology, Baylor College of Medicine, Houston, Texas, USA
[3]Dept. of Clinical Biochemistry, University of Cambridge, Cambridge, UK
[4]Neuroscience Program, University of Michigan, Ann Arbor, Michigan, USA
[5]Kresge Hearing Research Institute, University of Michigan, Ann Arbor, Michigan, USA
[6]Dept. of Psychiatry and Dept of Human Genetics, University of Michigan, Ann Arbor, Michigan, USA

*Received: 18 September 2002/Accepted: 1 November 2002*

***Abstract***

Mocha (*mh*), a mouse model for Hermansky-Pudlak syndrome (HPS), is characterized by platelet storage pool deficiency, pigment dilution, and deafness as well as neurological abnormalities. The trans-Golgi/endosome adaptor-related complex AP-3 is missing in *mh* mice owing to a deletion in the gene encoding the delta subunit. Mice mutant for a second allele, *mh*$^{2J}$, are as hyperactive as *mh*, and display both spike wave absence and generalized tonic clonic seizures, but have less coat color dilution, no hearing loss, and no hypersynchronized EEG. Here we show that the *mh*$^{2J}$ mutation is due to an IAP element insertion in the *Ap3d* gene leading to a C-terminally truncated protein. Despite correct assembly of the AP-3 complex and localization to the trans-Golgi network and endosomes, AP-3 function in neurons remains impaired. While *mh* mice show a severe reduction of vesicular zinc (TIMM staining) owing to mislocalization and degradation of the Zinc transporter ZnT-3, the TIMM and ZnT-3 staining patterns in *mh*$^{2J}$ varies, with normal expression in hippocampal mossy fibers, but abnormal patterns in neocortex. These results indicate that the N-terminal portion of the delta subunit is sufficient for AP-3 complex assembly and subcellular localization to the TGN/endosomes, while subsequent function is regulated in part by cell-specific interactions with the C-terminal portion.

Correspondence to: M. Burmeister; E-mail: margit@umich.edu
Present address for Prameela Kantheti: Center for Human Genetics, Institute of Bioinformatics and Biotechnology, Bangalore, India
Present address for Andrew Peden: Jenentech Inc., South San Francisco, Calif, USA.

***Introduction***

Oculocutaneous hypopigmentation accompanied by platelet storage pool deficiency (SPD) is found in humans [Hermansky-Pudlak (HPS) and Chediak-Higashi Syndrome (CHS)] as well as more than a dozen mouse mutants (Swank et al. 2000). The common defect in these recessive genetic disorders is that certain subcellular organelles are not able to store and transport their contents to their destinations. Consequently, melanosomes are smaller and fewer in number and contain less melanin, renal lysosomes show reduced secretion of their enzymes (Novak and Swank 1979), and the dense (delta storage) granules of platelets are empty, resulting in blood clotting delay (Novak et al. 1984; Reddington et al. 1987). Genes involved in both the human and the mouse disorders have recently been identified (Anikster et al. 2001; Huizing et al. 2001; Suzuki et al. 2001; Swank et al. 2000). Most of these genes code for proteins of still unknown function. One exception is the well-characterized AP-3 complex that is mutated in Hermansky-Pudlak syndrome type 2 (Dell'Angelica et al. 1999), the mutant mice *mocha* and *pearl*, the Drosophila mutants garnet, ruby, carmine, and orange, and a subset of yeast vacuolar protein sorting mutants (summarized by Odorizzi et al. 1998).

The recessive mouse mutant mocha (*mh*) is a typical SPD mutant with coat and eye color dilution, reduced levels of renal lysosomal enzymes in the urine, and prolonged bleeding due to storage pool deficiency in the dense granules of platelets (Lane and Deol 1974; Swank et al. 1991). Like several

other, but not all, SPD mouse mutants, *mocha* mice have balance defects due to defective or missing otoliths, and hearing loss progressing to complete deafness by 3–6 months of age (Rolfsen and Erway 1984; Swank et al. 1991). In addition, *mocha* mice have other neurological abnormalities, including behavioral hyperactivity and a unique hypersynchronized 6–7 Hz electrocorticogram (Noebels and Sidman 1989). We previously reported that the *mocha* phenotype is due to a deletion in the gene encoding the delta subunit of the adaptor-related protein complex, AP-3, leading to premature truncation of the delta subunit and complete absence of the other subunits of the complex (Kantheti et al. 1998).

The AP-3 complex is a heterotetramer consisting of two large subunits, delta and beta, and two smaller subunits, mu and sigma (Odorizzi et al. 1998; Robinson and Bonifacino 2001; Simpson et al. 1997). AP-3 is localized to vesicles budding from the trans-Golgi network, TGN (Simpson et al. 1997), as well as to more peripheral membranes that are partially accessible to endocytosed proteins, suggesting that the complex may function in the transport between the TGN and an endosomal compartment (Robinson and Bonifacino 2001). The identification of AP-3 mutations in Drosophila eye color mutants (Lloyd et al. 1999; Mullins et al. 2000; Odorizzi et al. 1998), yeast (Cowles et al. 1997; Odorizzi et al. 1998), mice (Feng et al. 1999; Kantheti et al. 1998), and humans (Shotelersuk et al. 2000) established that AP-3 mediates the sorting of cargo from the TGN and endosomes to lysosomes and related organelles, including melanosomes and platelet-dense granules, in many species.

A second allele of mocha, $mh^{2J}$, was identified at The Jackson Laboratory. This mutant is more mildly affected, shows a different cortical excitability pattern with no persistent hypersynchronization but with episodes of spike-wave and tonic clonic seizures not seen in *mh* mice (Noebels and Sidman 1989 and unpublished observations). Here we report that the $mh^{2J}$ mutation is due to the insertion of an intracisternal A particle at an exon/intron boundary. This mutation leads to production of a C-terminally truncated protein as well as small amounts of normal protein resulting from splicing across the IAP insertion. We previously determined that the delta subunit is necessary for AP-3 complex assembly, since the missing delta subunit in *mh* mice leads secondarily to the absence of all other subunits (Kantheti et al. 1998). In contrast, we find that the C-terminally truncated delta subunit in $mh^{2J}$ is stable and able to correctly assemble and localize the AP-3 complex to the TGN and endosomes, indicating that the N-terminal half of the delta subunit is necessary and sufficient for early steps in complex formation. Despite this finding, nervous system function in the $mh^{2J}$ mutant remains impaired.

In neurons, one cargo of the AP-3 complex is the zinc transporter ZnT-3. Loss of normal trafficking of this molecule in *mh* leads to lack of zinc sequestration in synaptic vesicles determined by Timm staining (Kantheti et al. 1998), and thus both molecules are useful markers for the integrity of AP-3 function in neurons. In contrast to *mh*, analysis of the $mh^{2J}$ brain revealed a normal distribution of the zinc transporter ZnT-3 and vesicular zinc in hippocampal mossy fibers, but abnormal ZnT-3 accumulation in the soma of neurons and loss of vesicular zinc staining in neocortical synapses. The results reveal selective vulnerability of protein cargo pathways to AP-3 hypofunction in different neuronal populations, which may contribute to the variation in neuronal phenotypes seen in *mh* and $mh^{2J}$ mice.

## Materials and methods

***Mouse stocks.*** All stocks were obtained from The Jackson Laboratory (Bar Harbor, Maine). Animal experiments were reviewed and approved by the local UCUCA/ULAM committees. The $mh^{2J}$ allele arose on the C3H/HeJ stock at The Jackson Laboratory.

***Southern blot analysis.*** Genomic DNA from spleen was prepared with a salting out procedure (Miller et al. 1988) or purchased from The Jackson Laboratory. DNA samples (C3H/HeJ-$mh^{2J}$ and C3H/HeJ control) were digested with restriction enzymes, fractionated on a 1% agarose gel, and blotted onto HybondTM-$N^+$ (Amersham). Hybridization was carried out at 65°C for 24–48 h. The insert of IMAGE clone #405026, which spans the 3′ end of *Ap3d*, was used as a radioactively labeled probe. The blots were then washed at 65°C for 20 min three times with 0.2 × SSC containing 0.2% SDS. A1-kb ladder (Gibco-BRL, Gaithersburg, Md.) was used as a size marker.

***Northern blot analysis.*** Total RNA was isolated using Trizol reagent, following the manufacturer's protocols (Gibco-BRL). Poly $(A)^+$ RNA was separated by using PolyA-Tract (Promega, WI, USA). 2 μg of poly $(A)^+$ RNA was fractionated on a 1% formaldehyde agarose gel and transferred to HybondTM-N+ (Amersham). Hybridization was carried out for 1 h by using Express Hyb (Clontech, Palo Alto, Calif.) hybridization solution at 68°C. Blots were washed four times with 2 × SSC containing 0.05% SDS at room temperature for 10 min each, followed by two

washes with 0.1 × SSC containing 0.1% SDS at 50°C for 20 min each. RNA ladder (363–9488 bp) was from USB (Cleveland, OH). For AP-3 delta, the insert of IMAGE clone #405026, which spans the 3′ end of *Ap3d*, was used.

***Genomic PCR.*** Genomic PCR was performed on 50–100 ng of C3H/HeJ-$mh^{2J}$ and C3H/HeJ genomic DNA purchased from The Jackson Laboratory. Primers P15 and P16 from exons 21 and 23 (see below) were used in standard PCR conditions: Buffer 2 (AB Peptides, St. Louis, Mo.): 50 mM Tris-HCl pH 9.1, 16 mM ammonium sulfate, 3.5 mM. $MgCl_2$, and 150 μg/ml BSA, performed in the presence of 5% DMSO, with annealing at 56°C and extension for 5 min at 72°C. In addition, in order to amplify the long inserted fragment, enzymes with proofreading ability had to be used; either a 5:1 ratio of Klentaq:PFU (AB Peptides, St. Louis, Mo.; Stratagene, La Jolla, Calif.) or with ''Long Template Expand Taq polymerase (Hoffman LaRoche, Basel, Switzerland). PCR Products were then separated by agarose gel electrophoresis. Genomic sequence from the boundaries has been submitted to genbank as AF469668 and AF469670. We did not fully sequence the 5- to 6-kb insertion, and the size of the insertion is an estimate based on gel electrophoresis but is consistent with the typical size of IAP elements (Kuff and Lueders 1988).

***RT-PCR.*** 1 μg of poly $(A)^+$ RNA from brain was used to synthesize first-strand cDNA by using Superscript according to the manufacturer's protocol (Gibco BRL). PCR was performed (see text or legend for combinations) with the following primers, synthesized at the University of Michigan Oligonucleotide Core facility: P4 forward: 5′-ATGGCC TCAAGATGGTCAAG-3′; P8 reverse: 5′-CCAG CTC GCAGATGACATTA-3′. These primers correspond to positions 221–241 bases and 832–851 of the mouse *Ap3d* cDNA (NM_007460), although Primer P4 has a frameshift mutation because it was based on a sequence of a mouse EST, AA221402 which has a sequencing error. P15 forward: 5′-GAAGCTGC CTGTCCAGAAAC-3′; P16 reverse: 5′-CCTCTT CCCCTTTGAGAACC-3′, correspond to 2650–2669 and 2917–2936 bp of that sequence. Other primers used are as described in Kantheti et al. (1998). 1 μl of first-strand cDNA was used as template in 50-μl PCRs under the following conditions: 94°C denaturation for 1 min, 55°C annealing for 2 min, and 72°C extension for 2 min in 1 × TNK 50 buffer (10 mM Tris/HCl pH 9.2, 5 mM $NH_4Cl$, 1.5 mM $MgCl_2$, 0.01% gelatin, and 14.7 mM 2-mercapto-ethanol) containing 0.25 mM dNTPs and 1.0 U of Taq polymerase. RT-PCR products were analyzed on 1% agarose and visualized by ethidium bromide staining. RT-PCR fragments were gel-purified with Ultrafree MC: 0.45 μm and 30,000 NMWL filters (Millipore, Bedford, mass.) and directly sequenced at the University of Michigan Sequencing Core facility. cDNA sequences have been submitted to Genbank under the following accession numbers: AF469669, AF469671.

***Timm histochemistry.*** Adult $mh^{2J}/mh^{2J}$ and littermates +/+ control mice were used for vesicular zinc visualization and ZnT-3 immunohistochemistry. To visualize vesicular zinc, a modification of the Timm stain was used (Kantheti et al. 1998). Mice were anesthetized with a combined solution containing: ketamine, xylazine, and acepromazine (0.5–1 ml/kg/i.m.), then transcardialy perfused with 0.1 M sodium phosphate buffer (PB, pH 7.4), followed by a sodium sulfide solution (0.48% $Na_2S_9H_2O$ in 0.15 M phosphate buffer during 60 min, pH 7.4). The perfusion was continued with a solution of 1% paraformaldehyde in 0.1 M PB. The brains were removed and left overnight in a 30% solution of sucrose in the fixative solution. Coronal 20 μm frozen sections were mounted on slides and allowed to dry. Sections were developed in the dark for 60 min with an aqueous solution consisting of 60 ml of 50% gum arabic, 10 ml of sodium citrate buffer, 30 ml of 5.7% hydroquinone, and 0.5 ml of 17% silver nitrate. Slides were then rinsed in tap water for 5 min, dehydrated in graded ethanol, cleared briefly in xylene, and cover slipped with Permount.

***Immunohistochemistry.*** After an anesthetic overdose of Avertin, animals were perfused through the left ventricle with 0.1 M sodium phosphate buffer (PB, pH 7.4), and then with 4% paraformaldehyde diluted in PB (pH 7.4). Brains were removed, post-fixed overnight in the same fixative solution, and stored in 30% sucrose solution at 4°C for cryoprotection. Transverse 40-μ brain sections were cut from frozen blocks in a cryostat at −20°C and stored in Tris-buffered saline (TBS) (0.15 M NaCl, 0.1 M Tris-HCl, pH 7.4) at 4°C until processing for immunohistochemistry. The free-floating sections were treated with 1% $H_2O_2$ in TBS for 1 h to block endogenous peroxidase. After several rinses in TBS, the sections were treated with 3% BSA, 3% goat serum, and 0.25% Triton X-100 in TBS for 1 h to reduce nonspecific staining. Sections were rinsed in TBS and then incubated with an affinity-purified rabbit antibody specific for ZnT-3 (Palmiter et al. 1996; a generous gift of R. Palmiter), for 1 h at room temperature and then overnight at 4°C, diluted 1:200 in TBS containing 2% BSA, 1% goat serum, and 0.25% Triton X-100. Following rinses for

2 h in TBS, sections were incubated in biotinylated goat anti-rabbit IgG (diluted 1:200) for 2 h at room temperature, rinsed for 1 h in TBS, and then incubated in ABC following the procedure described by the manufacturer (Vectastain Elite ABC kit, Vector Laboratories). The peroxidase reaction was detected with a metal-enhanced diaminobenzidine reagent (Vector). Sections were rinsed in TBS, mounted onto gelatin-coated slides, air dried, dehydrated, and cover slipped from xylene. The specificity of immunolabeling was verified by controls in which the primary antibody was omitted.

***Immunoprecipitations.*** Control and $mh^{2J}$ tissues were homogenized in 1% Triton X-100, 50 mM Tris-HCl pH 7.4 and 150 mM NaCl. The detergent extracts were clarified by spinning for 15 min at 100,000 *g*. The extracts were incubated with 100 μl of 50% protein A sepharose beads for 1 h at 4°C. The preadsorbed extracts were incubated with affinity-purified anti-AP-3 antibodies for 1 h at 4°C. 100 μl of 50% protein A sepharose beads was added, and the mixture incubated for 1 h at 4°C. The beads were collected by centrifugation and washed five times with homogenization buffer. The samples were then boiled in SDS sample buffer, run on SDS polyacrylamide gels, and subjected to Western blotting.

***Immunofluorescence and tissue culture.*** Primary fibroblasts were generated by taking tissue from 1- to 3-day-old mice and physically disrupting the tissue with a pair of scissors. The remaining unused part of the body was used for genotyping by Southern blot analysis (*Hin*dIII digest, as described by Kantheti et al. 1998). The disrupted tissue was transferred into DMEM supplemented with 10% fetal calf serum, 100 U/mL penicillin, 100 μg/mL streptomycin, 2 mM L-glutamine, and 50 μM mercaptoethanol. Primary fibroblasts were trypsinised and transferred onto multiwell test slides and fixed with −20°C methanol for 5 min, followed by 30 s in −20°C acetone. The C-terminal polyclonal anti-δ antibody was generated against amino acids 757–1112 and expressed as a GST fusion protein. The antiserum was affinity-purified as previously described (Simpson et al. 1997). The N-terminal polyclonal anti-δ antibody (22–756) has been previously described (Simpson et al. 1997). The secondary antibody used was Alexa Flour 488 anti-rabbit IgG, obtained from Molecular Probes (Eugene, Ore.). The cells were viewed with an Axioplan fluorescence microscope (Zeiss, Inc., Thornwood, NY) fitted with a Micro Max CCD camera (Roper Scientific, Inc., Marlow, Buckinghamshire).

## Results

***$mh^{2J}$ is a phenotypically mild allele (hypomorph) of mh.*** $mh^{2J}$ arose at The Jackson Laboratory on the C3H/HeJ strain but has not been previously described. Unlike *mh* mice, which are difficult to breed owing to their behavior, $mh^{2J}$ mice are fertile and breed quite well, especially when maintained on a mixed background. We have performed several crosses during which we observed $mh^{2J}$ on its original background, C3H/HeJ, in an $F_2$ with C57BL/6J, and in a cross of that $F_2$ mix with CAST/Ei (Kantheti et al. 1998). The coat color of $mh^{2J}$ mice varies with background but is generally much closer to normal than that of *mh* (see Fig. 1). While *mh* mice typically become deaf by 3 months of age, several $mh^{2J}$ mice of mixed background were unaffected at ages of up to 1.5 years. Evoked auditory brain responses (ABRs) obtained at frequencies of 4,000, 10,000, and 20,000 were found to be not significantly different from ABRs of control littermates (data not shown). Otolith defects in homozygous *mh* mice result in abnormal circling behavior and typically produce a head tilt. This vestibular phenotype is dependent on the diet of the pregnant dams and is observed less frequently in $mh^{2J}$ (<<20%) than in *mh* mice (30–50%) (Rolfsen and Erway 1984). Interestingly, the apparent motor hyperactivity we observed in $mh^{2J}$ mice seemed at least as severe as in *mh* mutants. Neurophysiological studies of homozygous mutants have also shown that, in contrast to the hypersynchronized 6- to 7-Hz electrocorticogram of *mh* mice, $mh^{2J}$ display normally synchronized background rhythms with occasional spike-wave discharges (Noebels 1984; Noebels and Sidman 1989). Despite their more normally appearing background EEG rhythms, tonic-clonic behavioral seizures are frequently observed in $mh^{2J}$ mice, although these are far more rare in *mh* mice. In summary, non-neurological traits such as coat color dilution and fertility in $mh^{2J}$ mice are less severely affected than in *mh* mice, while neurological traits persist but are qualitatively quite different.

***$mh^{2J}$ is due to an IAP element insertion.*** To examine the nature of the mutation in the $mh^{2J}$ allele, genomic Southern blots, prepared from DNA from $mh^{2J}$ and C3H/HeJ control animals cleaved with several different restriction enzymes, were hybridized with probes generated by RT-PCR. After we initially detected a genomic DNA rearrangement in $mh^{2J}$ with several different enzymes (Kantheti et al. 1998), DNA from mutant and control animals was analyzed with several different rarer cutting restriction enzymes (Fig. 2A). Probes from

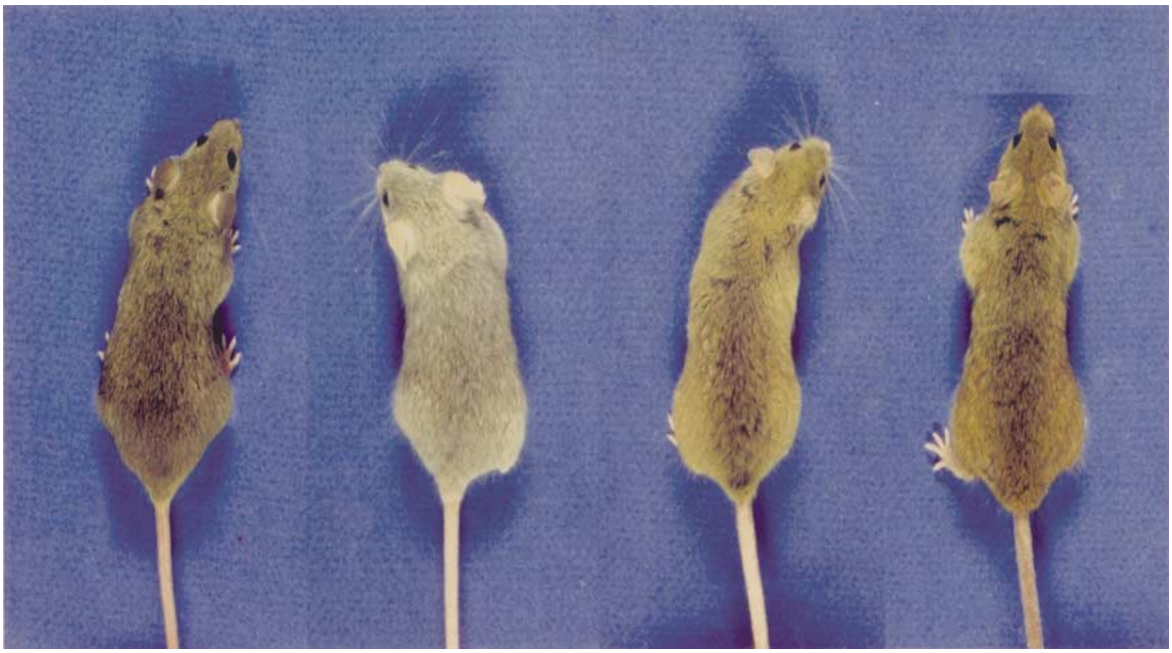

**Fig. 1.** Coat color of $mh^{2J}$ is only slightly diluted. Coats of (from left to right) *mh/gr* heterozygous control, mocha (*mh*), $mh^{2J}$ and $mh^{2J}$ heterozygote littermate control animals. All are on a mixed background. Note that it is not possible to use a +/+ control animal for *mh* because of the presence of a ''balancing'' grizzled (*gr*) allele, another coat color mutation, on the control chromosome owing to forced heterozygote maintenance of the line.

the middle of the *Ap3d* gene but not the 5′ end detected 4- to 64-kb larger DNA fragments in $mh^{2J}$, indicating that $mh^{2J}$ is likely due to an insertion in the center of the *Ap3d* gene. To determine the precise nature and location of this presumed insertion, we performed genomic PCR with primers from the central region of *Ap3d* (Fig. 2B). The resulting fragments are about 5–6 kb larger in $mh^{2J}$ than in the control DNA. The $mh^{2J}$-amplified fragment of P15/P16 was end sequenced. The sequence showed an insertion of an IAP element of the IΔ1 type into intron 21. IAP elements that have retrotransposed frequently have this structure, which contains a deletion of 1.9 kb of internal sequences (Kuff and Lueders 1988). The insertion resulted in a 6-bp target site duplication and was localized to the first 5 bp of the intron (see Fig. 4)

***Altered size and normal levels of Ap3d transcripts in $mh^{2J}$.*** To determine how the genomic insertion in the mutant affects *Ap3d* transcription, we performed Northern blot analysis using poly $(A)^+$ RNA from different tissues of mutant and control mice. While mRNA levels did not appear to be significantly different, the length of the major *Ap3d* transcript was found to be larger by about 2.0 kb (Fig. 3A). In the mutant kidney tissue, there is also a small amount of normal transcript that could not be detected in brain mRNA. In addition, all tissues examined showed small amounts of an even larger transcript. To determine the nature of the novel transcripts, RT-PCR analysis was performed on mutant and control brain poly$(A)^+$ RNA with primers spanning most of the *Ap3d* mRNA. Primers spanning the middle and 3′ end of the gene (P15+P16) yielded a fragment about 2 kb larger than the wild-type product in $mh^{2J}$, suggesting that a part of the IAP insertion is also transcribed (Fig. 2C). Sequence analysis shows that the major transcript results from two splicing events within the IAP element: one into and out of the first LTR element of the IAP insertion, the other in the middle of the IAP element. In addition to this major transcript containing part of the IAP element, we also found reduced levels of the normal mRNA product (Fig. 2C), although it was not detectable in brain on the Northern blot. Sequencing of this product confirmed that the sequence corresponded to wild type cDNA sequence. Fig. 4 summarizes the results of sequence analysis of genomic and major transcript sequences of mutant and wild type. Our results demonstrate that the major consequence of the IAP element insertion is an aberrant transcript, but a small amount of wild-type mRNA is also generated. The largest mRNA detected on the Northern blot could not be amplified or sequenced, but its size is consistent with a transcript containing most or all of the IAP element insertion.

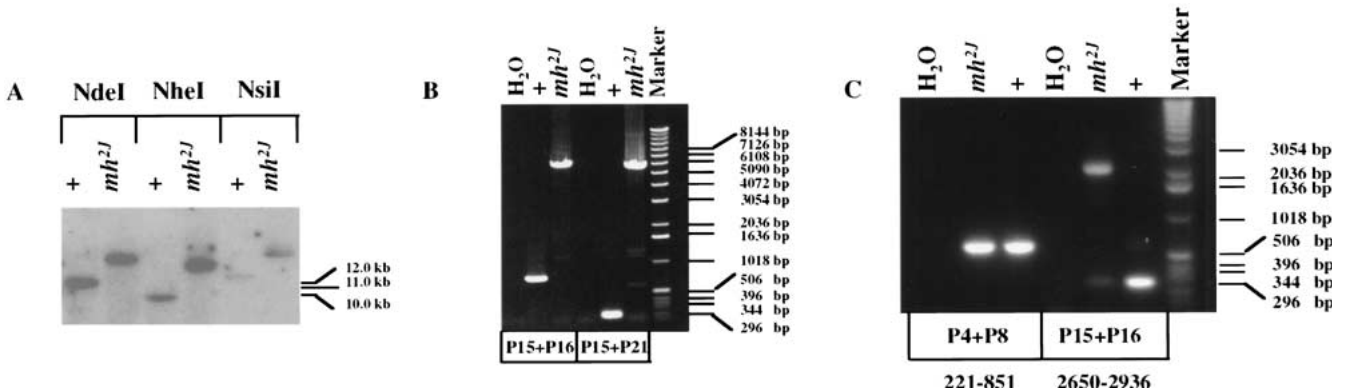


**Fig. 2.** $mh^{2J}$ is caused by an insertion in genomic DNA and in the transcript. **A**. A Southern blot was prepared by digestion of $mh^{2J}$ and C3H/HeJ (+) DNA with the restriction enzymes *Nde*I, *Nhe*I, and *Nsi*I, followed by hybridization with a probe to the *Ap3d* gene, and autoradiography. When choosing enzymes that cut as rarely as shown here, a pattern of increased fragment sizes in $mh^{2J}$ DNA is consistently observed. **B**. PCR was performed with primers in exons 21 and 23 on genomic DNA from $mh^{2J}$ and C3H/HeJ control (+) DNA. The results suggest an insertion of 5–6 kb $mh^{2J}$. **C**. mRNA was isolated from $mh^{2J}$ and control brains, followed by RT-PCR with primers in the 5′ region of *Ap3d* (P4+P8), and primers flanking the IAP element (P15+P16). PCR products were analyzed by agarose gel electrophoresis.

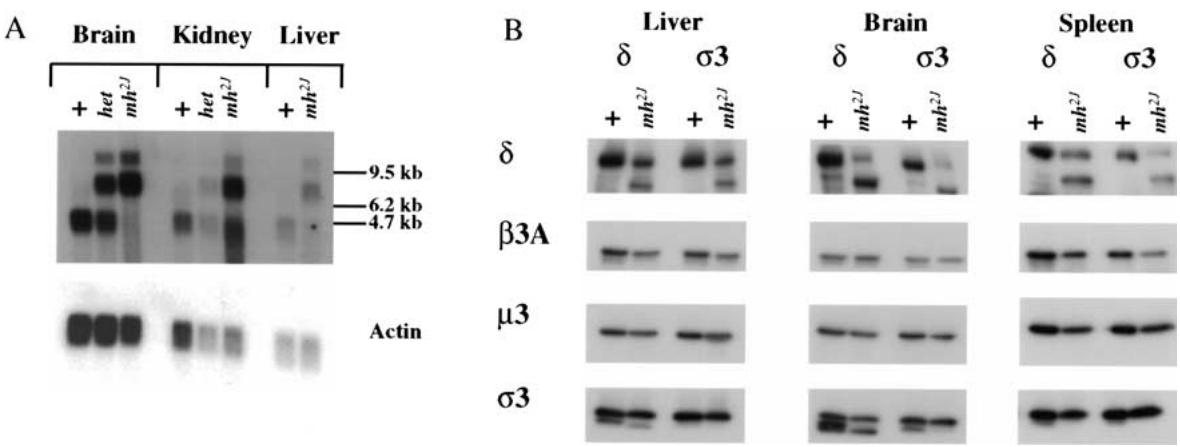


**Fig. 3.** $mh^{2J}$ tissues express a larger transcript resulting in a truncated protein form of the delta subunit. **A**. Northern blot analysis: 2 μg of mRNA from brains, kidneys, and liver of normal control littermates, heterozygous and $mh^{2J}$ mutant animals were loaded for a Northern blot and probed with the 3′ end of the murine AP-3 delta gene and submitted to autoradiography. Northern was stripped and rehybridized with a probe for actin. Sizes of selected bands of the size marker—stained separately—are indicated on the right. **B**. Native immunoprecipitations were performed from control (+) and $mh^{2J}$ liver, brain, and spleen tissue by using affinity-purified polyclonal antibodies against δ and σ3. The gels were Western blotted, and then appropriate regions were cut out and probed with the above antibodies as well as anti-β3 and μ3. The Western blots indicate that truncated and wild-type δ subunits are present in $mh^{2J}$ tissues and that the truncated δ subunit is able to incorporate into AP-3 complexes.

***Truncated AP-3 delta protein is correctly localized and participates in AP-3 complex formation.*** AP-3 is a heterotetrameric complex consisting of four subunits, two large (delta and beta) and two small (mu and sigma). Previously, we demonstrated that when the delta subunit is missing (as is the case in *mh* mice), the whole complex is absent, indicating that the delta subunit constitutes a ''linchpin'' essential for AP-3 complex formation and/or maintenance (Kantheti et al. 1998). In $mh^{2J}$, the major transcript containing a partial IAP element contains a stop codon (TAA) one amino acid after the insertion, predicting the production of a truncated AP-3 delta protein of 858 amino acids instead of the usual 1198 (857 of normal protein plus one additional amino acid). To examine whether this protein, predicted to have the ''trunk'' domain but not the C-terminal ''ear'' domain of AP-3 (Robinson and

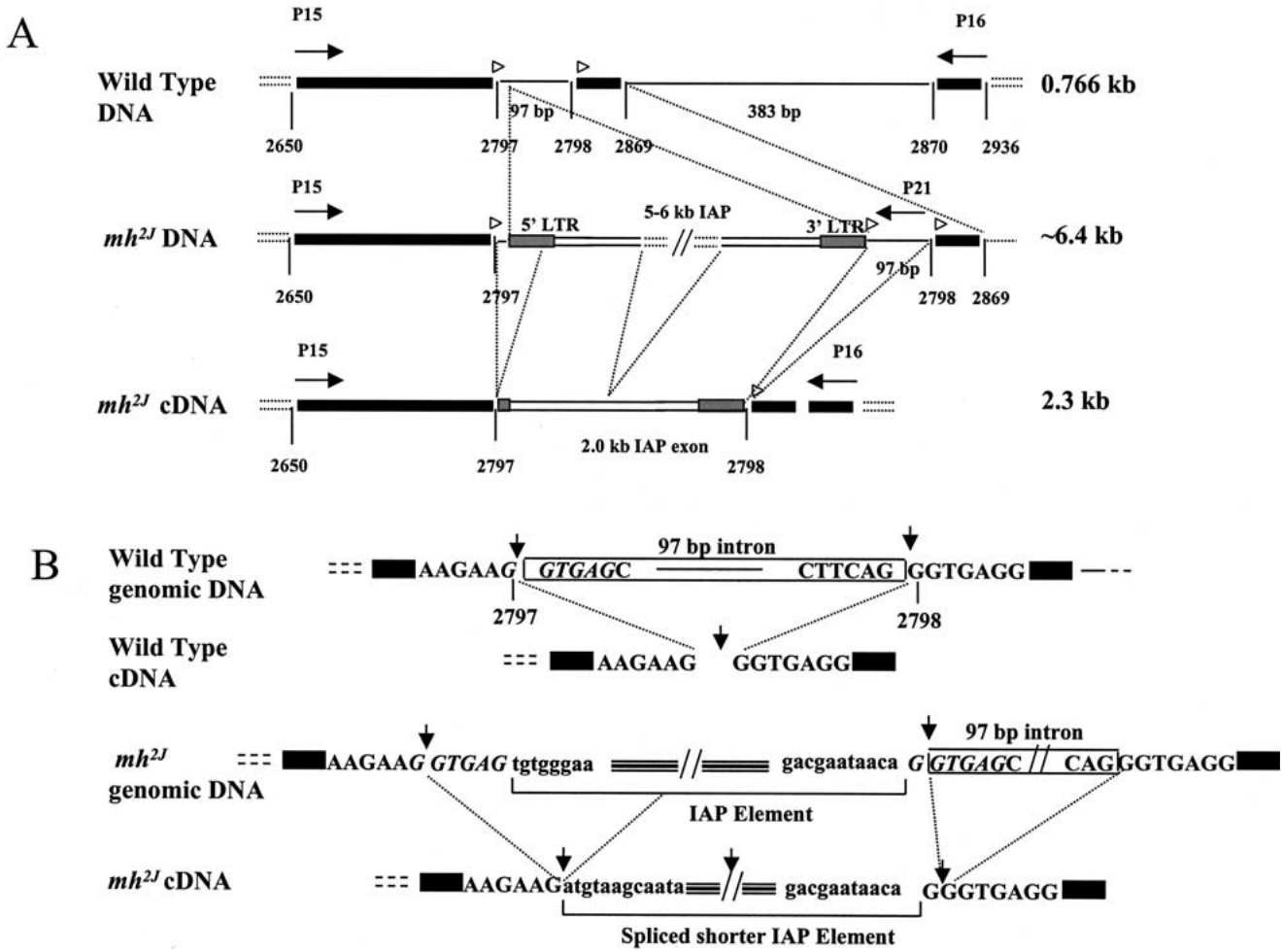


**Fig. 4.** Structure of the IAP element insertion and its transcription. **A**. Normal genomic context of exons 21 through 23. In $mh^{2J}$ genomic DNA, a 5- to 6-kb IAP element with LTRs at both ends is inserted in intron 21. In the cDNA, introns 21 and 22 are spliced, as well as a part of the IAP element. To the right, product sizes with PCR primers P15+P16 are indicated. An empty triangle symbolizes the sequence GGTGAG which is at the beginning of the 97-bp intron and the beginning of the next exon, and was duplicated at the target site of the IAP element insertion in $mh^{2J}$. **B**. Close-up of the sequences around the IAP insertion is shown. Duplicated target site is shown in italics. Arrows show exon-intron and exon-exon junctions respectively. All sequences were deposited in Genbank (AF469668, AF469669, AF469670, AF469671).

Bonifacino 2001) has retained some partial function, we performed immunoprecipitations with antibodies against AP-3 delta and against AP-3 sigma, followed by Western blotting against each of the four subunits. Figure 3B shows that both the normal and the truncated protein can clearly be detected, can be immunoprecipitated with both sigma and delta antibodies, and all other subunits are also present. These results indicate that the truncated AP-3 delta protein can participate in complex formation and maintenance. Together with our previous results on *mh* (Kantheti et al. 1998), these results indicate that the N-terminal half of AP-3 delta is vital for AP-3 complex formation and/or maintenance. However, the truncated protein may be less stable since the ratio of truncated to normal protein is much more favorable for the normal protein than the ratio of transcripts seen on the Northern blot, where the normal transcript is only barely detectable (compare Fig. 3A, B).

To investigate where a complex formed with truncated AP-3 delta protein is localized intracellularly, we performed immunofluorescence with two antibodies, an N-terminal antibody that is expected to recognize the normal and the truncated protein and a C-terminal antibody to amino acids after the predicted stop codon. Indeed, in $mh^{2J}$ fibroblasts (Fig. 5), there is very little protein found with the C-terminal antibody. In contrast, when the N-terminal antibody is used, punctuate perinuclear staining indiscernible from normal AP-3

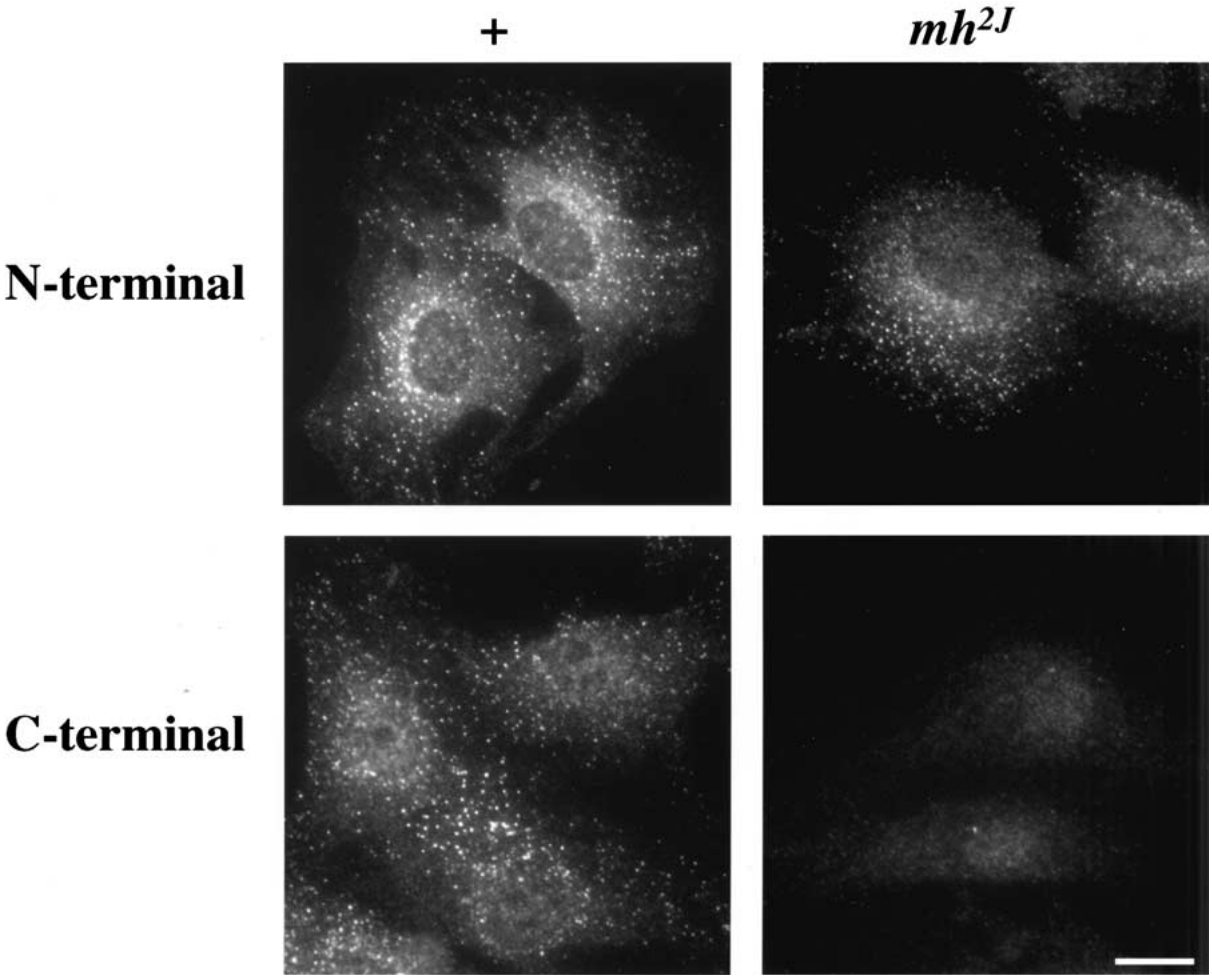


**Fig. 5.** Immunofluorescence localization of the δ subunit in $mh^{2J}$ and control flbroblasts (+). Primary flbroblasts were fixed with methanol and acetone and stained with affinity-purified polyclonal antibodies raised against either the N (22–756aa) or C (757–1112aa)-terminus of the δ subunit. The staining in $mh^{2J}$ cells indicates that the truncated δ subunit incorporates into complex, and this complex is able to be recruited onto membranes giving a staining pattern very similar to that observed in control flbroblasts. The reduced staining observed in the $mh^{2J}$ cells with the C-terminal antibody indicates that there is very little wild-type δ subunit present in these cells, (Scale bar 20 μm).

staining is observed (Fig. 5). This result suggests that once the complex is formed, it is correctly localized, and the C-terminal domain of the delta subunit is not crucial for correct intracellular localization.

***Synaptic vesicular zinc patterns are normal in $mh^{2J}$ hippocampal mossy fibers but not in neocortical fibers.*** The *mh* mutant was previously shown to display a striking loss of vesicular zinc within widespread brain regions linked to abnormal trafficking of the vesicular zinc transporter protein ZnT-3 (Kantheti et al. 1998). The Timm method was used to examine the localization patterns of vesicular zinc in the $mh^{2J}/mh^{2J}$ brain. In the hippocampus (Fig. 6A, B), the mossy fiber pathway showed intense staining in both +/+ $mh^{2J}/mh^{2J}$. In contrast, the light staining normally present in the strata oriens (SO) and radiatum (SR) of +/+ is entirely absent in $mh^{2J}/mh^{2J}$ hippocampus. This pattern of Timm stain was observed along the entire hippocampal septotemporal axis. Similar differences were also observed in other brain regions, reflecting a widespread loss of zinc-rich vesicles within the neuropil. In the neocortex (Fig. 6C, D), the staining of zinc-containing axonal boutons commonly seen in laminae II–III and V of +/+ mice is also reduced in the $mh^{2J}/mh^{2J}$ brain. A reduction of vesicular zinc was also observed in entorhinal cortex and amygdala of the mutant mouse (data not shown). These

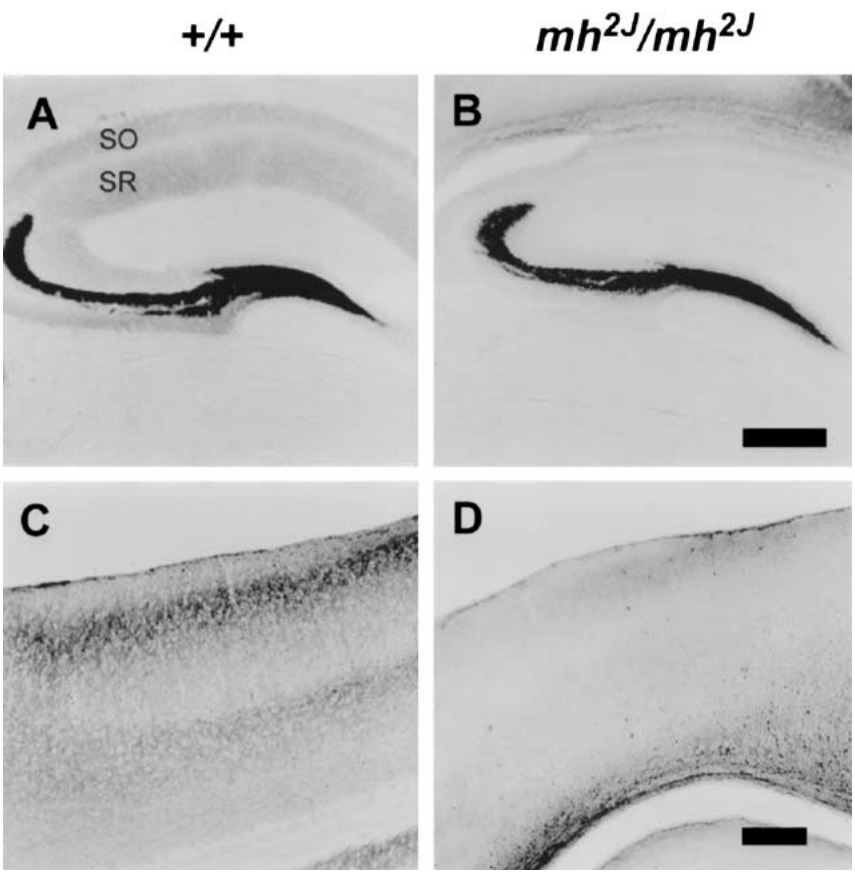


**Fig. 6.** Selective vulnerability of vesicular zinc patterns in $mh^{2J}$ neocortex and hippocampus. Timm staining in adult $mh^{2J}$/$mh^{2J}$ (**B, D**) and in +/+ (**A, C**) hippocampus reveals normal staining pattern of zinc-filled synaptic vesicles $mh^{2J}$ mutant mossy fiber axons, but absence of light staining over the stratum oriens (SO) and stratum radiatum (SR) layers. C and D: loss of Timm staining in superficial and deep layers of frontal neocortex in $mh^{2J}$/$mh^{2J}$ mice. Calibration bar (A, B), 500 μm; (C, D), 200 μm.

findings demonstrate that the $mh^{2J}$ mutation differentially affects zinc sequestration within axons in different brain regions.

***ZnT-3 transporter trafficking is altered in $mh^{2J}$ neurons.*** An affinity-purified polyclonal antibody to ZnT-3 was used to evaluate the distribution of the zinc transporter ZnT-3 in the brain of $mh^{2J}$ mice (Fig. 7). In the dentate granule cells of the hippocampus, immunoreactivity for ZnT-3 in axons was present in both +/+ and $mh^{2J}$/$mh^{2J}$ mice (Fig. 7A, 7B), and the mossy fiber bundle was intensely stained in the mutant mice. This finding is consistent with the normal appearance of Timm-stained, zinc-filled vesicles described above. In contrast, in widespread areas of the cerebral cortex, the homogeneous immunostaining present in the neuropil of +/+ (Fig. 7C, E) is slightly decreased in the brain of $mh^{2J}$/$mh^{2J}$ (Fig. 7D, F); however, intense cytoplasmic staining of large, pyramidal-shaped cells in these regions indicates that ZnT-3 abnormally accumulates in the soma and proximal dendrites of these cells, a finding never observed in the wild-type control brains. These findings are congruent with those described above showing lack of Timm staining in cortical fibers.

## Discussion

We have demonstrated that the $mh^{2J}$ allele of *Ap3d* is a hypomorph that is less severely affected in all non-neurological phenotypes. In $mh^{2J}$ mice, both low levels of normal AP-3 and larger amounts of abnormal AP-3 are formed. The ratio of normal to abnormal protein is lowest in brain tissue. While it is tempting to speculate that there is a rough correlation between less normal protein in brain than in other tissues, the neurological phenotypes being relatively more severe, there are also other possible explanations. Neurological effects are background dependent, and we currently cannot compare *mh* mice and $mh^{2J}$ mice on the same genetic background, and, therefore, the phenotypic differences may in part be due to genetic background effects.

Is the mutant AP-3 complex functional? While the mutant complex is formed and located in the correct subcellular compartment, it seems not to be able to function properly. Heterozygous *mh*/+ mice are completely normal, yet are expected to have about 50% of AP-3. $mh^{2J}$ fibroblasts seem to have fairly high levels of (mutant) AP-3, but a much re-

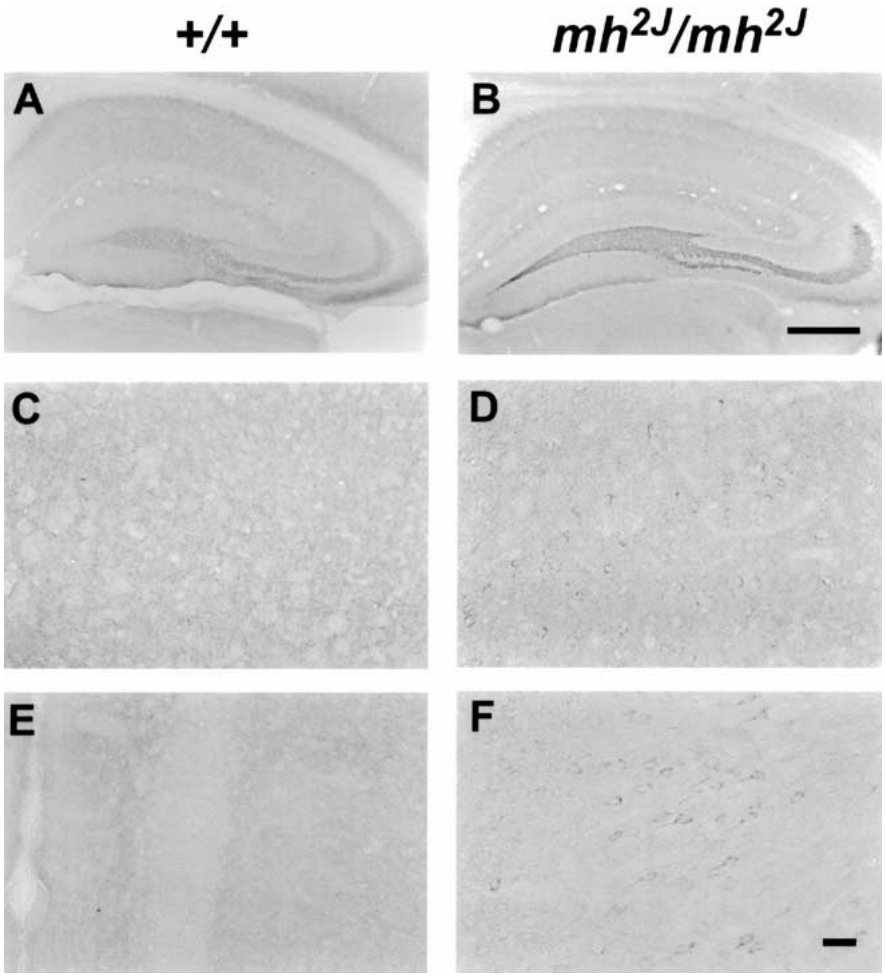


**Fig. 7.** ZnT-3 is correctly sorted in $mh^{2J}$ hippocampus but not neocortex. Immunohistochemistry for ZnT-3 reveals distribution of zinc transporter in +/+ and $mh^{2J}/mh^{2J}$ mouse brain. In the hippocampal formation, mossy fibers (dentate granule cell axons) are strongly stained in both the +/+ (**A**), and mutant (**B**) owing to their high content of synaptic vesicles containing ZNT-3 and zinc. Cell body layers in the dentate gyrus are unstained. In neocortex, +/+ somas remain unstained; however, in $mh^{2J}/mh^{2J}$ brain there is clear and aberrant staining of cell somas (dense pericentric cytoplasmic staining) in frontal (**C, D**) and cingulated (**E, F**) cortical regions, consistent with a lack of trafficking of ZNT-3 synaptic vesicles into the axons, as shown by decrease of zinc-stained axons in cortex. Calibration bar (A, B), 400 μm; (C, D, E, F), 30 μm.

duced level of normal AP-3. Thus, the milder nonneuronal phenotypes of $mh^{2J}$ mice can be best explained by the small amount of remaining normal AP-3. Neurologically, $mh^{2J}$ mice are quite severely affected, and there is little or no normal AP-3 in brain. This conclusion is also consistent with another mutation in AP-3, in the pearl mouse which is caused by mutations in *Ap3b1*, one of the beta subunits of the AP-3 complex. The first allele of pearl described, caused by decreased and aberrant transcripts (Feng et al. 1999), is clearly milder than the subsequently reported knock-out mouse (Yang et al. 2000). Thus, very small amounts of normal AP-3 can already have phenotypic consequences in making the phenotype significantly milder.

Our finding here shows that the N-terminal domain of the AP-3 delta protein is sufficient for assembly and TGN location, but not for correct sorting, is supported by experiments in tissue culture of the similar beta domain (Peden et al. 2002). For the beta subunit, as we report here for the delta subunit, removal of the C-terminal ear domain results in correct complex assembly and localization to membranes, but no correct sorting of lysosomal membrane proteins. The C-terminal domains in some other adaptins bind other proteins (Owen et al. 2000), and it seems it is this function that is importantly missing in $mh^{2J}$. But because $mh^{2J}$ has both a relatively highly abundant abnormal protein and small amounts of normal protein, we cannot say whether the milder phenotype, i.e., residual function, is due to the small amount of normal protein or to some residual function of the abnormal protein. In Drosophila, the homolog of AP-3 delta is mutated in flies with the garnet mutation of which several alleles have been described (Lloyd et al. 1999). While mocha is a complete null, and there are several Drosophila null alleles, a mild allele in Drosophila, the $g^3$ allele, seems to be similar to $mh^{2J}$ in that a C-terminally truncated protein is produced from a shorter transcript (Ooi et al. 1997). But the exact sequence is unknown, and just as in $mh^{2J}$, there a is a minor larger transcript, so it is unclear whether there is a minor larger protein made in $g^3$ or not.

### Acknowledgments

We thank Gary Dootz, Shannon Carskadon, Kathleen Pottman and Damaris Sufalko for assistance, and Richard Palmiter for the ZnT-3 antibody. This work was supported by the National Institutes of Health (NS32130, M.Burmeister; NS29709, HD24064 J.L.Noebels), and by the Wellcome Trust (M.S.Robinson).

### References

1. Anikster Y, Huizing M, White J, Shevchenko YO, Fitzpatrick DL et al. (2001) Mutation of a new gene causes a unique form of Hermansky-Pudlak syndrome in a genetic isolate of central Puerto Rico. Nat Genet 28, 376–380
2. Cowles CR, Odorizzi G, Payne GS, Emr SD (1997) The AP-3 adaptor complex is essential for cargo-selective transport to the yeast vacuole. Cell 91, 109–118
3. Dell'Angelica EC, Shotelersuk V, Aguilar RC, Gahl WA, Bonifacino JS (1999) Altered trafficking of lysosomal proteins in Hermansky-Pudlak syndrome due to mutations in the beta 3A subunit of the AP-3 adaptor. Mol Cell 3, 11–21
4. Feng L, Seymour AB, Jiang S, To A, Peden AA et al. (1999) The beta3A subunit gene (Ap3b1) of the AP-3 adaptor complex is altered in the mouse hypopigmentation mutant pear1, a model for Hermansky-Pudlak syndrome and night blindness. Hum Mol Genet 8, 323–330
5. Huizing M, Anikster Y, Gahl WA (2001) Hermansky-Pudlak syndrome and Chediak-Higashi syndrome: disorders of vesicle formation and trafficking. Thromb Haemostasis 86, 233–245
6. Kantheti P, Qiao X, Diaz ME, Peden AA, Meyer GE et al. (1998) Mutation in AP-3 delta in the mocha mouse links endosomal transport to storage deficiency in platelets, melanosomes, and synaptic vesicles. Neuron 21, 111–122
7. Kuff EL, Lueders KK (1988) The intracisternal A-particle gene family: structure and functional aspects. Adv Cancer Res 51, 183–276
8. Lane PW, Deol MS (1974) Mocha, a new coat color and behavior mutation on chromosome 10 of the mouse. J Hered 65, 362–364
9. Lloyd VK, Sinclair DA, Wennberg R, Warner TS, Honda BM et al. (1999) A genetic and molecular characterization of the garnet gene of *Drosophila melanogaster*. Genome 42, 1183–1193
10. Miller SA, Dykes DD, Polesky HF (1988) A simple salting out procedure for extracting DNA from human nucleated cells. Nucleic Acids Res 16, 1215
11. Mullins C, Hartnell LM, Bonifacino JS (2000) Distinct requirements for the AP-3 adaptor complex in pigment granule and synaptic vesicle biogenesis in *Drosophila melanogaster*. Mol Gen Genet 263, 1003–1014
12. Noebels JL (1984) Isolating single genes of the inherited epilepsies. Ann Neurol 16, S18–21
13. Noebels JL, Sidman RL (1989) Persistent hypersynchronization of neocortical neurons in the mocha mutant of mouse. J Neurogenet 6, 53–56
14. Novak EK, Swank RT (1979) Lysosomal dysfunctions associated with mutations at mouse pigment genes. Genetics 92, 189–204
15. Novak EK, Hui SW, Swank RT (1984) Platelet storage pool deficiency in mouse pigment mutations associated with seven distinct genetic loci. Blood 63, 536–544
16. Odorizzi G, Cowles CR, Emr SD (1998) The AP-3 complex: a coat of many colours. Trends Cell Biol 8, 282–288
17. Ooi CE, Moreira JE, Dell'Angelica EC, Poy G, Wassarman DA et al. (1997) Altered expression of a novel adaptin leads to defective pigment granule biogenesis in the *Drosophila* eye color mutant garnet. EMBO J 16, 4508–4518
18. Owen DJ, Vallis Y, Pearse BM, McMahon HT, Evans PR (2000) The structure and function of the beta 2-adaptin appendage domain. EMBO J 19, 4216–4227
19. Palmiter RD, Cole TB, Quaife CJ, Findley SD (1996) ZnT-3, a putative transporter of zinc into synaptic vesicles. Proc Natl Acad Sci USA 93, 14934–14939
20. Peden AA, Rudge RE, Lui WW, Robinson MS (2002) Assembly and function of AP-3 complexes in cells expressing mutant subunits. J Cell Biol 156, 327–336
21. Reddington M, Novak EK, Hurley E, Medda C, McGarry MP et al. (1987) Immature dense granules in platelets from mice with platelet storage pool disease. Blood 69, 1300–1306
22. Robinson MS, Bonifacino JS (2001) Adaptor-related proteins. Curr Opin Cell Biol 13, 444–453
23. Rolfsen RM, Erway LC (1984) Trace metals and otolith defects in mocha mice. J Hered 75, 159–162
24. Shotelersuk V, Dell'Angelica EC, Hartnell L, Bonifacino JS, Gahl WA (2000) A new variant of Hermansky-Pudlak syndrome due to mutations in a gene responsible for vesicle formation. Am J Med 108, 423–427
25. Simpson F, Peden AA, Christopoulou L, Robinson MS (1997) Characterization of the adaptor-related protein complex, AP-3. J Cell Biol 137, 835–845
26. Suzuki T, Li W, Zhang Q, Novak EK, Sviderskaya EV et al. (2001) The gene mutated in cocoa mice, carrying a defect of organelle biogenesis, is a homolog of the human Hermansky-Pudlak syndrome-3 gene. Genomics 78, 30–37
27. Swank RT, Reddington M, Howlett O, Novak EK (1991) Platelet storage pool deficiency associated with inherited abnormalities of the inner ear in the mouse pigment mutants muted and mocha. Blood 78, 2036–2044
28. Swank RT, Novak EK, McGarry MP, Zhang Y, Li W et al. (2000) Abnormal vesicular trafficking in mouse models of Hermansky-Pudlak syndrome. Pigment Cell Res 13, 59–67
29. Yang W, Li C, Ward DM, Kaplan J, Mansour SL (2000) Defective organellar membrane protein trafficking in Ap3b1-deficient cells. J Cell Sci 113, 4077–4086